Development and Validation of a Navier-Stokes Code for Hypersonic External Flow

James Stevenson Ryan*
University of Colorado, Boulder, Colorado
Jolen Flores†
NASA Ames Research Center, Moffett Field, California
and
Chuen-Yen Chow‡
University of Colorado, Boulder, Colorado

A new computational fluid dynamics procedure, compressible Navier-Stokes (CNS), is developed for application to hypersonic vehicle design. The CNS code uses a zonal approach, which makes it unique from standard hypersonic codes. Some of the advantages of this approach are that it alleviates the difficulties of grid generation for complex configurations, improves computational efficiency, allows incorporation of component parts, and permits grid refinement as needed. This zonal capability will allow the modeling of the external flowfield of vehicles from tip to tail. An equilibrium air model is also an available option. Validation cases include a comparison of ideal gas results with experimental data on a simple vehicle geometry at Mach 10.3 and 15-deg angle of attack. The equilibrium real-gas model is tested against published computations on a sphere cone at Mach 20.53 and 5-deg angle of attack. Computational results show good to excellent agreement with experiment and code-to-code comparisons. Grid refinement effects on skin friction and heat transfer are also documented for the sphere-cone case.

Introduction

UNTIL recently, much of the work in applied computational fluid dynamics has focused on the subsonic, transonic, and supersonic flight regimes. However, a renewed interest in hypersonic and aerothermodynamics has been sparked by recently proposed space transportation systems.[1,2] In the design of hypersonic vehicles, the use of experimental facilities is limited because of the high flow enthalpies and high speeds required to model these flowfields. Therefore, useful experimental results for the full flight regime of a hypersonic vehicle are difficult or impossible to obtain in current experimental facilities. Only a limited range of Mach and Reynolds numbers can be obtained in current facilities,[3] and the highest values are obtainable only for very small models. Because of these limitations, hypersonic aerodynamics will rely on computational fluid dynamics (CFD) for design. The same experimental limitations make it difficult to obtain data for the validation of the CFD codes, which are now being developed. These circumstances have led to the use of both experimental and computational data for compressible Navier-Stokes (CNS) validation.

Because of the extremely high temperature of the stagnation and combustion regions around these vehicles, the air will be partially dissociated. Therefore, in attempting to predict the heating environment, the assumption of a perfect gas with constant properties will be inadequate. The influence of real-gas effects must be accounted for in the numerical solution. Significant flowfield differences (compared with ideal gas) will exist, affecting shock-layer thickness,[4,5] heat-transfer rates, and the composition of the air. The flowfield differences indicated will also alter the aerodynamics of the hypersonic configuration.[6]

Codes that simulate three-dimensional hypersonic flow with an equilibrium air capability are currently available. For example, Balakrishnan et al.[4] uses a central-difference algorithm coupled with an equilibrium air model to simulate real-gas flowfields. Edwards[7] ran the same code but with the viscous option. The code of Bhutta et al.[8] is a space-marching code coupled with an equilibrium air model. These codes are well documented and have been used successfully to simulate the real-gas viscous and inviscid flow about three-dimensional geometries.

However, none of the mentioned codes is currently set up to handle complicated geometries and the associated problems. A procedure to aid in the design of hypersonic vehicles not only must account for real-gas effects but, for complex vehicles, must address problems with grid generation and integration of the propulsion system. Zonal schemes have proven to be successful in simulating flows over complicated geometries.[9-11] The CNS code was developed with this in mind and in support of the National Aero-Space Plane.[12,13] The CNS code solves the unsteady, thin-layer, Navier-Stokes equations in three dimensions with real-gas effects for complex configurations. CNS uses a zonal approach to alleviate the problems of grid generation about complex vehicles. This same zonal approach will allow easy implementation of propulsion system interfaces, combustion codes, and convergence acceleration techniques.[14]

The zonal approach also makes it easy to interface CNS with other flow solvers.[15] CNS provides solutions for entire flowfields, but solutions over complex vehicles may be unacceptably expensive for design purposes. Space-marching procedures such as upwind parabolized Navier-Stokes (UPS) are

Presented as Paper 89-1839 at the AIAA 9th Computational Fluid Dynamics Conference, Buffalo, NY, June 14-16, 1989; received July 21, 1989; revision received Aug. 31, 1989.

*Research Assistant, Department of Aerospace Engineering Sciences. Student Member AIAA.
†Research Scientist. Member AIAA.
‡Professor, Department of Aerospace Engineering Sciences. Associate Fellow AIAA.

much less expensive but they require an accurate starting solution,[15] and regions with streamwise separation cannot be solved. By transferring information between the two procedures at zonal interfaces, accurate, nose-to-tail calculations can be obtained much more efficiently.

Code Development

The current version of CNS is derived from two earlier codes. The flow solver is F3D[16], a two-factored, partially flux-split, three-dimensional, thin-layer Navier-Stokes algorithm. Flux splitting is applied in the streamwise direction, and central differencing is used in the crossflow directions. As a consequence of the central differencing in the normal and crossflow directions, numerical dissipation terms are employed. They are given as combinations of second and fourth differences. In the vicinity of shock waves, the fourth-difference terms can cause oscillations; therefore, it is desirable to drop these terms and rely only on the second-difference terms, but only in the vicinity of the shock. A pressure sensor effectively reduces the fourth-difference influence and increases the second-difference term near the shock. Away from the shock, the fourth difference dominates. The F3D algorithm uses the standard Baldwin-Lomax turbulence model. The solver was originally developed for transonic applications and has been extensively applied in that regime,[16] as well as at higher Mach numbers.[17] The version of F3D used in CNS also includes an equilibrium air model based on the curve fits of Srinivasan et al.[18] Those curve fits are valid for temperatures up to 25,000 K and for densities from 10^{-7} to 10^{3} amagats (ρ/ρ_0).

The zonal interface logic is derived from the transonic Navier-Stokes (TNS) code.[9] The success of that method for complex vehicle configurations has been extensively demonstrated in transonic calculations.[10,11] Through zoning, areas of interest within a grid may be refined without rebuilding the entire grid. Also, complex geometries may be modeled by assembling grids about each simpler component rather than by attempting to grid the entire body in a single pass. This strategy also enables the use of different equation sets for different regions in a single run. For example, areas away from the body may be zoned separately, and the Euler equations may be used. Zones with insignificant real-gas effects may revert to the ideal-gas equations. Convergence may be accelerated by selecting a different time-step size for each zone (for steady-state calculations). Central processing unit (CPU) time may also be saved by turning off iterations in upstream zones that are already converged. Another advantage of zoning is that the zone size may be tailored to suit the memory capabilities of available computers.

The overlapping of zones is controlled by the user. Zones in the streamwise direction are usually overlapped by one cell. Zonal interfaces parallel to the body, with a viscous zone on the body surface and an inviscid zone wrapped around it, are overlapped by several cells. Information is transferred between the zones and involves either injection or at most a two-dimensional interpolation. These interfaces are not conservative and effectively lag the interior grid points by one time step. However, the explicit updating of the zonal boundaries has not proven to be a problem.

The boundary conditions are applied as follows. At the outer boundary, freestream conditions are applied throughout the iteration process. At the outflow boundary, a simple zeroth-order extrapolation of the conservative variables is used. On the surface of the geometry, the standard no-slip condition is applied, with the density (and hence total energy) computed using either the ideal or equilibrium real-gas option. On the surface one can specify either adiabatic conditions or a fixed wall temperature.

The CNS code is capable of running on the Cray 2, Cray X-MP, and Cray Y-MP machines. Memory requirements are about 4 million words for a grid whose largest zone contains 150,000 points. Additional zones do not require additional main memory as they are transferred to SSD or disk when not in use. Solutions on the sphere-cone case described below required about 5 h of Cray 2 time on a single CPU for 3- to 4-orders-of-magnitude drop in the L-2 norm on a grid of 118,800 points. The code runs between 90 and 120 μs per grid point per iteration. Choosing grid dimensions close to the Cray vector length of 64 was found to reduce the CPU requirements. In fact, the extent to which the chosen array dimensions lend themselves to vectorization is more important to the speed than which machine is used.

Validation

Two test cases have been chosen for validation of the CNS code. The CNS code has computed solutions for more complicated geometries[19] and for other cases using classified designs.[20] However, for purposes of the grid refinement study and its effect on heat transfer and skin friction, the sphere-cone case was chosen. The hypersonic vehicle was chosen since experimental data (albeit only pressure data) was generated in support of the NASP project as was the development of the CNS code.

The computational data used for comparison is from a sphere-cone case published by Bhutta et al.[8] These data have the advantage of providing detailed information for the entire flowfield. Detailed numerical results for the sphere-cone case have been provided by Lewis[21] to supplement the published plots.

The experimental data used for comparison are those of Lockman et al.[22] The experiment uses a simplified hypersonic vehicle geometry, and test conditions cover Mach numbers from 5 to 10 and angles of attack from 0 to 15 deg.

Sphere-Cone Validation

The sphere-cone case selected is one of several published by Bhutta et al.[8] The body has a nose radius of 4.572 cm (0.15 ft). It is 30 nose radii long and has a 7-deg half-angle. The published case was calculated using a separate viscous shock-layer scheme to provide a starting solution for an iterative parabolized Navier-Stokes (PNS) solver (PNSEQ3D). The flow conditions are shown in Table 1. Laminar flow and symmetry about the pitch plane are assumed. The Reynolds number is based on nose radius. The wall temperature is fixed at 2000 K.

Table 1 Flow conditions for sphere-cone case (equilibrium real gas)

Altitude, m	24,000
Mach number[a]	20.53
Reynolds number	8.63×10^5
Density,[a] kg/m^3	0.0445
Temperature,[a] K	219.5
Velocity, m/s	6100
Angle of attack, deg	5

[a]CNS primary inputs.

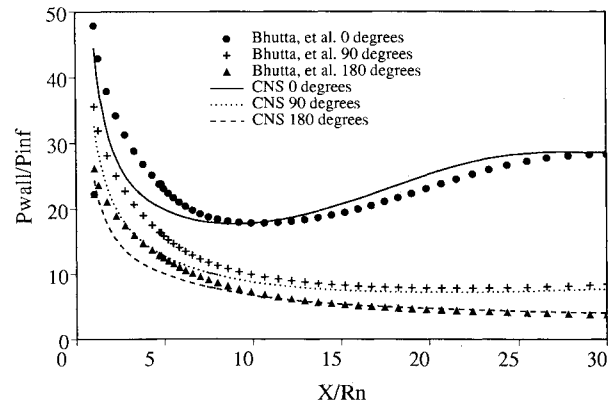

Fig. 1 Normalized pressure along the cone at three circumferential stations.

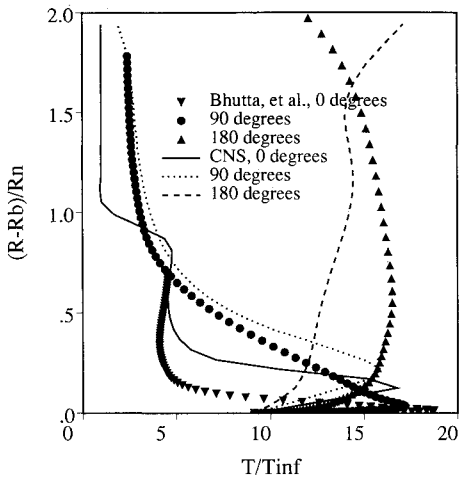

Fig. 2 Temperature in the flowfield at the end of the sphere-cone at three circumferential locations, base grid computation.

In each case, an equilibrium air model is used. The curve fits due to Srinivasan et al.[18] were used in CNS, and a table lookup procedure was used in the PNSEQ3D code.

Several quantities are selected for comparison in validating CNS against the Bhutta et al. results. Pressure, heat transfer, and skin friction are considered along three lines running the length of the sphere cone. Those lines are located at the windward symmetry plane (0 deg), planform plane (90 deg), and leeward symmetry plane (180 deg). In addition, the temperature in the flowfield is examined along lines extending radially from the end of the sphere cone at the same three circumferential angles.

The first quantity examined was surface pressure (see Fig. 1). CNS calculates lower pressures than reported by Bhutta et al. along the forward portion of the cone. The present results are consistent in calculations on a variety of grids, but no evidence is available to indicate which solution is in error.

To consider more than just surface quantities, the temperature in the flowfield was examined. This quantity provided an indication of how important appropriate grid refinement is to this problem. On the original grid of 60 (axial or streamwise) $\times$ 60 (normal) $\times$ 33 (circumferential) points, the inaccurate results shown in Fig. 2 were obtained. A lack of appropriate grid refinement was suspected. Rather than simply adding points, the computational grid was modified to capture the regions of interest in the flowfield more efficiently. The symmetrical outer boundary of the base grid was moved inward to reduce the number of points outside the bow shock. The interior points were reclustered along the existing radial grid lines. The resulting grid is shown in Fig. 3. This grid greatly improved the results on the windward side of the body, as shown in Fig. 4. After this modification, only the lee symmetry plane showed large discrepancies from the Bhutta et al. results.

Further detailed examination of the flowfield revealed that the inflections in the leeward temperature profile were caused by a vortex separating from the cone at 13.2 nose radii from the tip. The CNS zonal capability was used to explore the separation region by the use of a local zone that could be refined independently. The zonal approach permitted these refinements to be made with minimal impact on the overall memory requirements and saved computational time by retaining the same forebody solution for all cases. Studies on this grid revealed that the separation was grid dependent and was physically incorrect. A nonzonal type of code would not have allowed this type of analysis to be accomplished. If physical intuition or comparisons to other CFD or experimental results suggest an error in the flowfield, the zonal scheme allows more detailed analysis by its ability to refine the zone locally. The temperature profiles were particularly sensitive to refinements

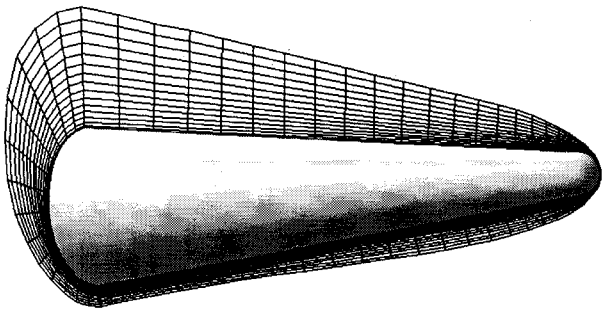

Fig. 3 Sphere-cone computational grid with modified outer boundary. Actual grid is finer than shown.

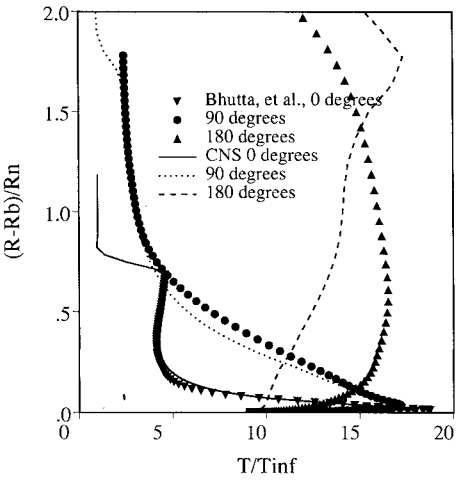

Fig. 4 Temperature in the flowfield at the end of the sphere-cone at three circumferential locations, modified grid computation.

in the body-normal direction. It was also seen that local refinement in the separation region was not adequate. Errors still propagated into the refined region from the coarser regions upstream.

The final grid configuration was based on the original modified-outer-boundary grid. The axial and circumferential spacing remained the same. To improve the distribution of points in the boundary layer, the number of points in the body-normal direction was increased to 99, and the grid was split into two zones. After splitting, each zone consisted of 101,277 points; 31 axial, 99 normal, and 33 circumferential.

To accurately calculate surface-measurable quantities, the boundary layer must be resolved over the whole body. Control of the first-point spacing is the most important factor in achieving this resolution. To evaluate the spacing, y^+ values were calculated for all points adjacent to the sphere-cone surface. The y^+ was defined as

$$y^+ = \left(\frac{\rho U_t \Delta y}{\mu}\right)^{1/2}$$

where U_t is the flow speed tangent to the body, and Δy is the normal distance from the wall to the adjacent grid point. Even though y^+ is normally used for turbulent flows, it is also a good indicator of grid resolution for laminar cases such as this one. These y^+ calculations were integrated into the grid modification program, allowing the capability to produce grids with appropriate normal spacing over the entire body surface.

The first point off of the body in the earlier grids had a constant normal spacing of 1×10^{-6}, which resulted in a wide range of y^+ values. Although the average y^+ was not excessive, the errors generated in regions of high y^+ propagated throughout the flowfield. For the new grid, the normal spacing

was adjusted to give a y^+ value of approximately 0.2 at all locations on the body. After the grid adjustment, the solution was reconverged. The y^+ values along the windward symmetry planes of the two grids are compared in Fig. 5 along with values for a later grid with a target y^+ of 0.08. The values for all three circumferential stations on the 0.2 y^+ grid are shown in Fig. 6. Note that these changes were achieved in a single pass of the grid program without iteration. The new grid remained constant during reconvergence of the solution, so that the final y^+ was not constant, especially at the nose. Reconvergence of the solution requires about half as much time per grid point as a solution from freestream.

The normal spacing in the new grid with 0.2 y^+ target varied over a range of 1×10^{-7} to 2×10^{-6}. With the new constant y^+ grid, good results were obtained. Temperatures at the end of the body nearly matched the Bhutta et al. results except in a small portion of the lee side flow (see Fig. 7). Figure 7 also shows that the shock at the 0- and 90-deg locations was captured much more sharply than before, as can be seen from the slope of the curves where the temperature drops to freestream.

The new grid improved the heat-transfer results dramatically (see Fig. 8). Heat transfer and skin friction show excellent correlation over most of the body, as shown in Figs. 9 and 10. The only substantial discrepancies are seen in the nose region, where the skin friction at $X/Rn \approx 0.5$ varies from the Bhutta et al. results. The heat transfer also differs at this

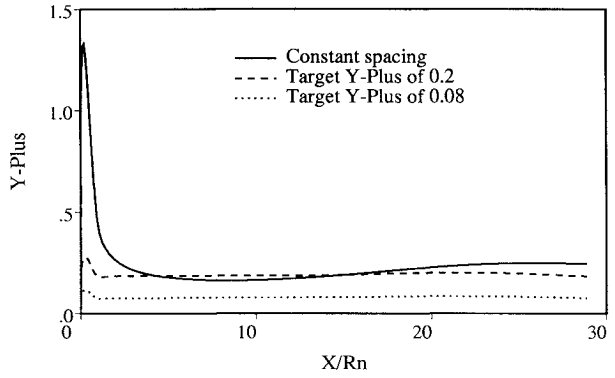

Fig. 5 Values of y^+ for grids with and without y^+ control. The windward station is shown.

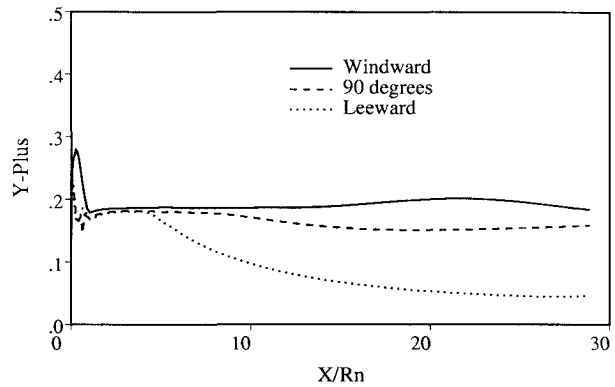

Fig. 6 Values of y^+ resulting from a target y^+ of 0.2.

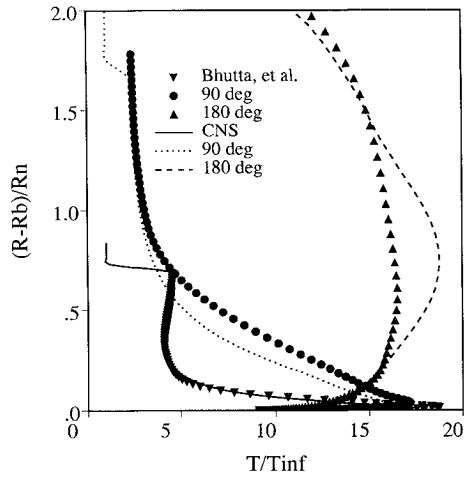

Fig. 7 Temperature in the flowfield at the end of the sphere-cone (target $y^+ = 0.2$).

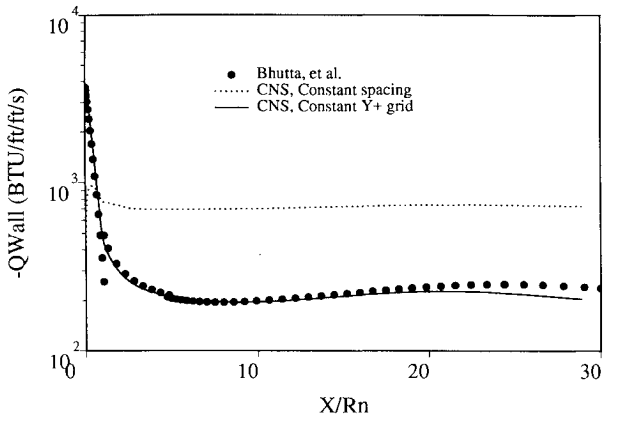

Fig. 8 Heat transfer for constant-wall-spacing and constant-y^+ grids (windward plane only).

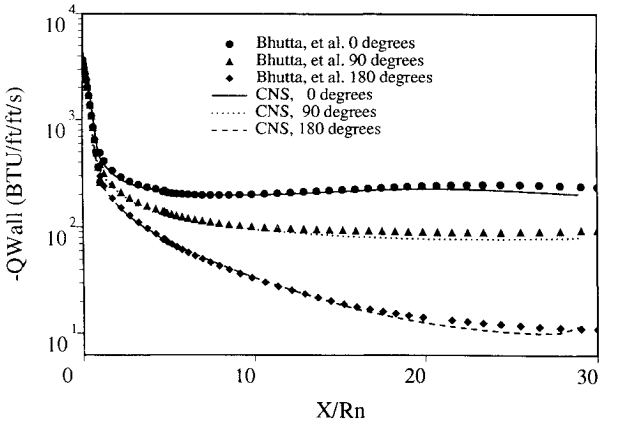

Fig. 9 Heat-transfer comparison (target $y^+ = 0.2$).

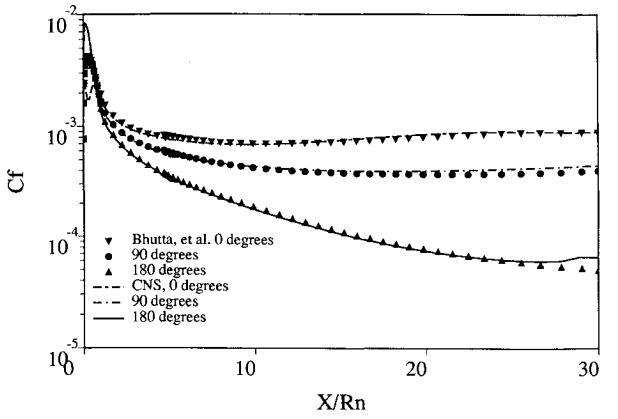

Fig. 10 Skin-friction comparison (target $y^+ = 0.2$).

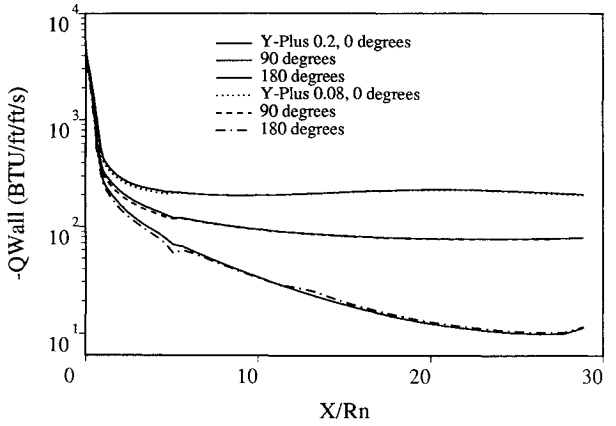

Fig. 11 Heat transfer calculated by CNS on the two y^+ modified grids showing grid independence.

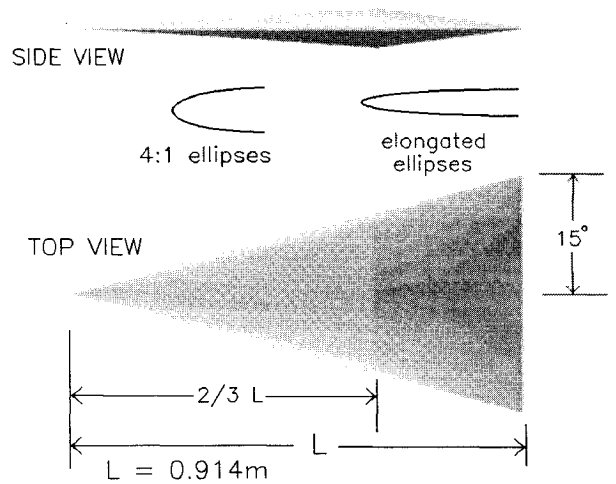

Fig. 12 All-body definition.

location, although it is not visible in the plot. The deviations may be explained by the jump in y^+ values at that location (see Fig. 6).

The grid independence of these results has been verified by restretching the grid points to achieve a y^+ of about 0.08 for most of the body. The wall heat transfer is compared to the previous result in Fig. 11.

Validation on the Ames All-Body

Lockman et al.[22] have obtained data in the Ames 3.5-ft hypersonic wind tunnel, which is useful for code validation. The model is a simple hypersonic vehicle shape known as the "all-body." The all-body has an elliptical cone forebody, followed by an afterbody that flattens and widens to a line at the tail (see Fig. 12).

The available data include pressure distributions for Mach 10.3 at $\alpha = 0$ and 15 deg. The higher angle-of-attack case, $\alpha = 15$ deg, has been selected for this paper. Earlier computational validation based on the all-body includes the comparison of results from four codes in Edwards et al.[23] Comparisons between experimental and computational results have been made for several of the flow conditions by Lockman et al.[22]

The base grid for the all-body is shown in Fig. 13. It is generated using a hyperbolic grid generator and spans a large enough computational region to accommodate flows for a wide range of Mach numbers and angles of attack. After modification of the outer boundary to closely accommodate the shock for this case, it takes the form shown in Fig. 14. This modification provides much more efficient use of the points in

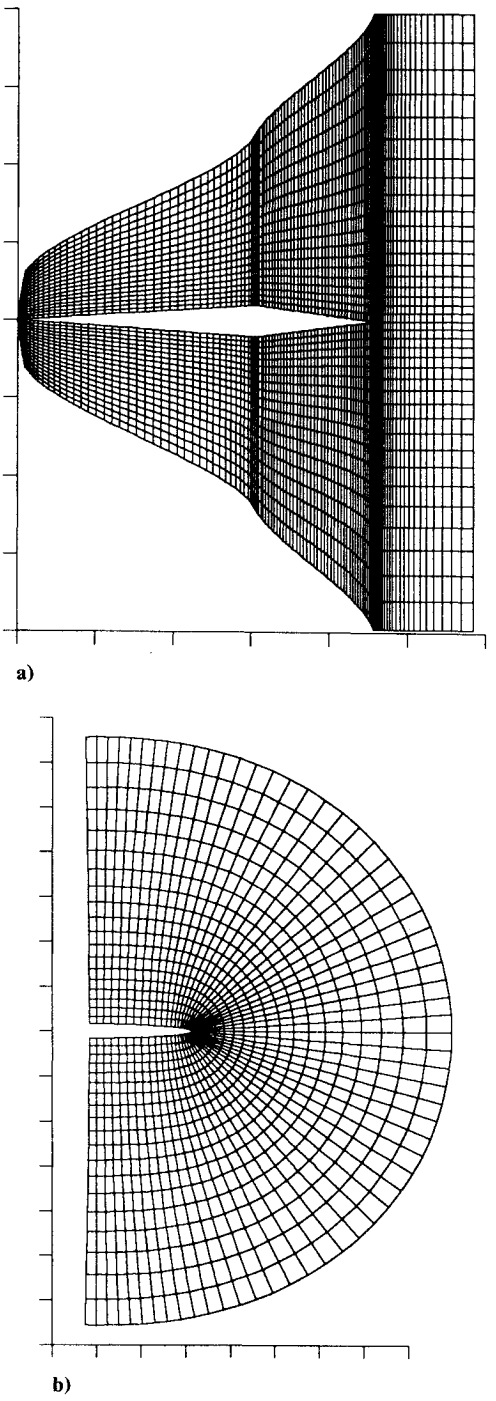

Fig. 13 All-body base grid. Actual grid is finer than shown: a) symmetry plane, b) cross section at $X/L = 0.87$.

the computational grid. The improvement in results provided by this procedure has been described previously for the sphere-cone case. The final grid used for the all-body calculations comprised eight zones, each with 58 radial points and 63 circumferential points. The zones were stacked sequentially in the axial direction with a total of 194 axial stations. The grid contained 708,876 points and required about 45 CPU hours on the Cray Y-MP to converge. The points in this grid were not efficiently distributed in either the axial or the circumferential directions, and the zone sizes were far from optimal for vectorization; therefore a much faster solution is possible. Another improvement in speed is available from convergence acceleration. Using a nonlinear over-relaxation method, Cheung et al.[14] have achieved improvements of about 35% for a two-zone CNS calculation.

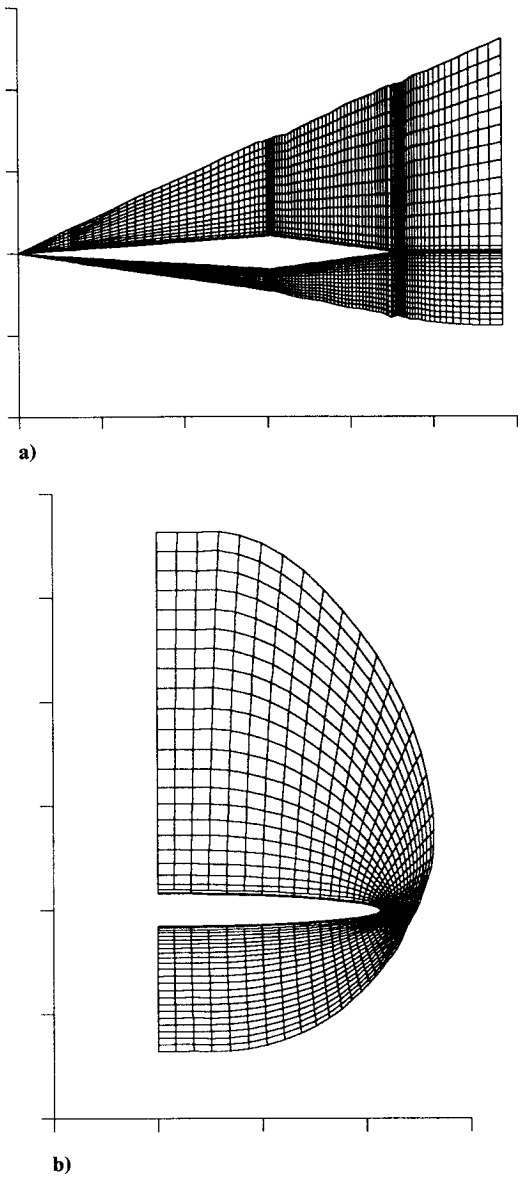

Fig. 14 All-body grid with modified outer boundary. Actual grid is finer than shown: a) symmetry plane, b) cross section at $X/L = 0.8$.

The experimental data consist of surface pressures along the body centerline and around the body at several axial stations. The CNS calculations are made using ideal-gas assumptions, and the Baldwin-Lomax turbulence model is used along the entire body. The Reynolds number of 15×10^6 based on body length supports the assumption of turbulent flow, but the extent of turbulent or transitional flow in the experiment will not be known until more detailed data are available. Additional flow parameters are shown in Table 2. Figure 15 shows the coefficient of pressure around a cross section at a streamwise station of $X/L = 0.4$. The results on the forebody show excellent agreement with the experimental data. Figure 16 shows the results at two stations on the afterbody, $X/L = 0.7$ and $X/L = 0.95$. On the afterbody, the $X/L = 0.95$ station

Table 2 All-body case flow conditions, ideal gas

Mach number[a]	10.3
Reynolds number[a]	5×10^6
Density,[a] kg/m^3	0.0445
Angle of attack, deg	15

[a]CNS primary inputs.

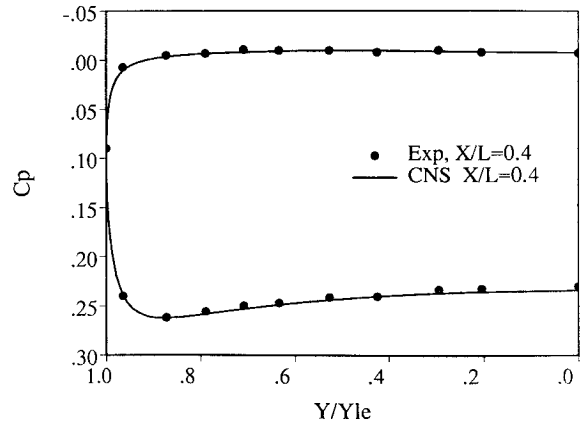

Fig. 15 Pressure coefficient distribution around the all-body (forebody).

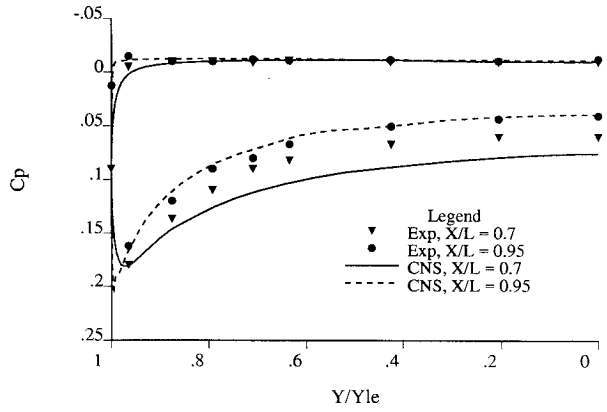

Fig. 16 Pressure coefficient distribution around the all-body (afterbody).

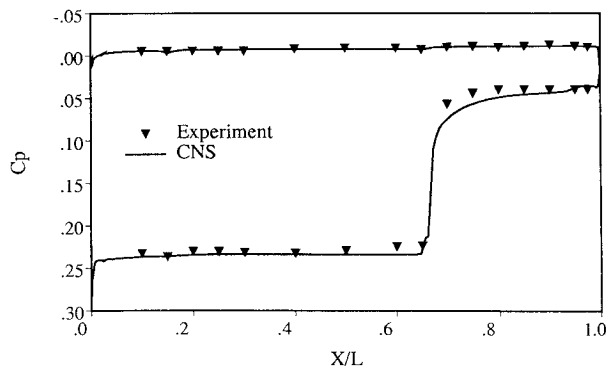

Fig. 17 Pressure coefficient along the all-body centerline.

shows very good agreement, but the $X/L = 0.7$ station shows an overprediction of the pressure coefficient on the windward side of the body. This station is located just 3.4% of the body length behind the transition from forebody to afterbody where the surface angle makes a sharp change. Lack of grid resolution at the transition appears to be responsible for the error, which is confined to the windward side of the body where a large expansion occurs. Another view of the transition between forebody and afterbody is provided by Fig. 17. The results are excellent, except just behind the windward expansion.

Summary

A new solution procedure known as CNS is developed. The strength of the CNS code is in its zonal scheme. The advantages of this zonal scheme are the ability to model complex geometries, to locally refine zones where needed, to allow the implementation of CNS on different computers with limited memory, and to allow the solution of different equation sets in different zones for computer efficiency. The current capabilities of the procedure include modeling of the entire external flow about hypersonic vehicle shapes from a captured shock at the nose to the beginning of the wake. Ideal-gas and equilibrium air models are implemented.

Validation using the sphere-cone data shows good solution accuracy for the surface pressure and flowfield temperature. The accuracy of heat-transfer and skin-friction calculations is excellent over the major part of the geometry. At the nose region, the comparisons are good. Control of spacing normal to the body must be applied over the entire body surface in order to achieve accurate results. When a y^+ of 0.2 or less is used with CNS, boundary-layer resolution is adequate to produce excellent results. In addition, a method has been developed to adapt the grid to boundary-layer properties, insuring adequate resolution of the wall gradients.

Comparisons to the Ames all-body pressure data show good general agreement. Eight zones were used for this calculation. In general, no difficulty was experienced in convergence or accuracy due to the interfacing of the zones. For future validation using the all-body geometry, experimental data will be needed for quantities other than surface pressure.

Acknowledgments

This work was partially supported under NASA Ames Research Center Grant NCC 2-440. Computational resources were provided by the Numerical Aerodynamic Simulation Facility at NASA Ames. Dr. Clark Lewis provided tabulated results for the sphere-cone case described here and in Ref. 21.

References

[1]Walberg, G. D., "A Survey of Aeroassisted Orbit Transfer," *Journal of Spacecraft and Rockets*, Vol. 22, No. 1, 1985, pp. 3–18.

[2]Howe, J. T., "Introductory Aerothermodynamics of Advanced Space Transportation Systems," *Journal of Spacecraft and Rockets*, Vol. 22, No. 1, 1985, 104–111.

[3]Diewert, G. S., "Aerothermodynamics Research at NASA Ames," *Aerodynamics of Hypersonic Lifting Vehicles*, AGARD CP-428, April 1987, pp. 24-1 to 24–17.

[4]Balakrishnan, A., Davy, W. C., and Lombard, C. K., "Real Gas Flowfield About Three-Dimensional Configurations," AIAA Paper 83-0581, Jan. 1983.

[5]Balakrishnan, A. and Davy, W. C., "Viscous Real Gas Flowfields About Three-Dimensional Configurations," AIAA Paper 83-1511, June 1983.

[6]Maus, J. R., Griffith, B. J., Szema, K. Y., and Best, J. T., "Hypersonic Mach Number and Real Gas Effects on Space Shuttle Orbiter Aerodynamics," AIAA Paper 83-0343, Jan. 1983.

[7]Edwards, T. A., unpublished results.

[8]Bhutta, B. A., Lewis, C. H., and Kautz F. A., II, "A Fast Fully-Iterative Parabolized Navier-Stokes Scheme for Chemically Reacting Reentry Flows," AIAA Paper 85-0926, June 1985.

[9]Holst, T. L., Thomas, S. D., Kaynak, U., Gundy, K. L., Flores, J., and Chaderjian, N. M., "Computational Aspects of Zonal Algorithms for Solving the Compressible Navier-Stokes Equations in Three Dimensions," *Numerical Methods in Fluid Mechanics I*, edited by K. Oshima, Inst. of Space and Astronautical Science, Tokyo, 1985, pp. 113–122.

[10]Flores, J., Reznick, S. G., Holst, T. L., and Gundy, K. L., "Transonic Navier-Stokes Solutions for a Fighter-Like Configuration," AIAA Paper 87-0032, Jan. 1987.

[11]Flores, J., Chaderjian, N. M., and Sorenson, R. L., "Simulation of Transonic Viscous Flow over a Fighter-Like Configuration Including Inlet," AIAA Paper 87-1199, June 1987.

[12]Ryan, J. S., Flores, J., and Chow, C.-Y., "Hypersonic Flow Simulations about the All-Body Configuration Using a Zonal Approach," Fourth National Aero-Space Plane Technology Symposium, Monterey, CA, Paper 92, Feb. 1988.

[13]Flores, J., Ryan, J. S., and Edwards, T. A., "CNS Code Development," Fifth National Aero-Space Plane Technology Symposium, Hampton, VA, Paper 12, Oct. 1988.

[14]Cheung, S., Cheer, A., Hafez, M., and Flores, J., "Convergence Acceleration of Viscous and Inviscid Hypersonic Flow Calculations," AIAA Paper 89-1875, June 1989.

[15]Lawrence, S., Tannehill, J., and Kaul, U., "UPS Code Enhancements," 6th National Aero-Space Plane Symposium, Paper 16, April 1989.

[16]Ying, S. X., Steger, J. L., Shiff, L. B., and Baganoff, D., "Numerical Simulation of Unsteady, Viscous, High-Angle-of-Attack Flows using a Partially Flux Split Algorithm," AIAA Paper 86-2179, Aug, 1986.

[17]Rizk, Y. M., Chaussee, D. S., and Steger, J. L., "Numerical Simulation of the Hypersonic Flow around Lifting Vehicles," NASA TM-89444, April, 1987.

[18]Srinivasan, S., Tannehill, J. C., and Weilmuenster, K. J., "Simplified Curve Fits for the Thermodynamic Properties of Equilibrium Air," ISU-ERI-Ames-86401, June 1986.

[19]Edwards, T. A. and Flores, J., "Toward a CFD Nose-to-Tail Capability: Hypersonic Unsteady Navier-Stokes Code Validation," AIAA Paper 89-1672, June 1989.

[20]Edwards, T. A. and Lawrence, S. L., "CFD Analysis of NASP Forebody Flowfields," NASP Technical Module Review, JPO, Air Force Wright Aeronautics Lab., Dayton, OH, April 1989.

[21]Lewis, C. H., private communication, Jan. 24, 1989.

[22]Lockman, W. K., Cleary, J. W., and Lawrence, S. L., "Flow Visualization and Pressure Distributions for an All-Body Hypersonic Aircraft," Fourth National Aero-Space Plane Technology Symposium, Monterey, CA, Paper 53, Feb. 1988.

[23]Edwards, T. A., Chaussee, D. S., Lawrence, S. L., and Rizk, Y. M., "Comparisons of Four CFD Codes as Applied to a Hypersonic All-Body Vehicle," AIAA Paper 87-2642, Aug. 1987.

Clark H. Lewis
Associate Editor